Applied Surface Science 314 (2014) 558–563

Contents lists available at ScienceDirect

Applied Surface Science

journal homepage: www.elsevier.com/locate/apsusc

# Theoretical study of $SO_2$ adsorption on goethite (1 1 0) surface

Carolina E. Zubieta[a,*], Leandro F. Fortunato[b], Patricia G. Belelli[a], Ricardo M. Ferullo[b]

[a] IFISUR, CONICET and Universidad Nacional del Sur, Av. Alem 1253, Bahía Blanca, Argentina
[b] INQUISUR, CONICET and Universidad Nacional del Sur, Av. Alem 1253, Bahía Blanca, Argentina

ARTICLE INFO

*Article history:*
Received 8 April 2014
Received in revised form 23 June 2014
Accepted 24 June 2014
Available online 14 July 2014

*Keywords:*
FeOOH
$SO_2$
Adsorption
Density functional calculations
Surface vacancies

ABSTRACT

Adsorption of $SO_2$ on fully hydrated and partially dehydrated (1 1 0) surface of goethite (α-FeOOH) has been investigated using density functional theory (DFT) and periodic conditions. Different degrees of dehydration were modeled by eliminating one or two water molecules from the fully hydrated surface. Calculations indicate that $SO_2$ shows preference to adsorb on dehydrated surface and the transformation to surface sulfite, bisulfite and sulfate was observed. In particular, surface sulfite can be formed over a variety of different dehydrated surfaces as monodentate and bidentate complexes. Theoretical vibrational frequencies of all the species have also been computed. Taking into account all the structures, we found frequency values within the 650–1030 $cm^{-1}$ region due to S—$O_{Fe}$ stretching, and between 1010 and 1190 $cm^{-1}$ due to S—O stretching. Furthermore, monodentate mononuclear and bidentate binuclear sulfite complexes present distinctive features at low frequencies (600–700 $cm^{-1}$).



## 1. Introduction

Iron oxides and oxyhydroxides have been object of numerous studies because of their technological importance in different areas such as corrosion and catalysis. They present high affinity with an important variety of contaminants and nutrients and as a result they play an important role in environmental processes [1]. Their efficient adsorbent role of organic and inorganic species makes them a big potential material for industrial applications. Goethite (α-FeOOH) is a common constituent of surface water sediments and soils, and it is one of the most important components of aerosol particles present in the atmosphere.

Sulfur dioxide is one of the main components of air pollution and smog. Its transport and transformation is an important environmental objective because of its capacity to form acid rain with the consequent environmental and human health effects. This gas is toxic and irritating, affecting the mucous membranes and respiratory system. Therefore, the process of $SO_2$ conversion to other sulfur-containing compounds of lower risk is highly desirable. The interaction of $SO_2$ with oxide surfaces is of great interest owing to different reasons. For instance, metal oxides have been investigated as adsorbents to clean industrial emissions of $SO_2$ [2]. On the other hand, atmospheric aerosol particles can act as substrates to catalyze the $SO_2$ oxidation in the troposphere, an important topic in relation with the formation of acid rain [3].

The adsorption of $SO_2$ over a wide variety of materials has been previously reported [3–14]. Zhang et al. have studied the irreversible $SO_2$ adsorption on different oxides to form sulfite, bisulfate and sulfate species [4]. They observed a high reactivity with FeOOH in comparison with other oxides such as $Al_2O_3$, MgO, $Fe_2O_3$ and MgO. Furthermore, surface-active oxygen and hydroxyl on the particles were found to be the key factors to the conversion of $SO_2$ to sulfite, bisulfate and sulfate surface species. Site-blocking experiments with bases and acids on alumina show that strong chemisorption of $SO_2$ occurs on basic sites, whereas acidic sites seem to be responsible for weak adsorption [5].

The oxidation of $SO_2$ in the presence of $O_2$ on different iron oxides was also studied by using diffuse reflectance infrared Fourier transform spectroscopy (DRIFTS) [6]. The results revealed adsorption bands between 1000 and 1300 $cm^{-1}$ on α-FeOOH and α-$Fe_2O_3$ assigned to the stretching motion of adsorbed sulfate on the surface. Baltrusaitis et al. by using X-ray photoelectron spectroscopy (XPS) have observed that $SO_2$, in the absence of $H_2O$ and $O_2$, adsorbs preferentially as sulfite on goethite and hematite, although evidences for adsorbed sulfate was also found [7]. In the presence of $O_2$, adsorption of $SO_2$ on hematite resulted in the formation of sulfate with no detectable sulfite species. In the case of goethite, there was an increase in the amount of sulfate in the presence of $O_2$, but the predominant surface species remained sulfite. Interestingly, Kaneko and Matsumoto found that highly crystalline goethite exhibits higher chemisorption ability for $SO_2$ [8].

* Corresponding author. Tel.: +54 0291154710377.
*E-mail address:* czubieta@uns.edu.ar (C.E. Zubieta).

http://dx.doi.org/10.1016/j.apsusc.2014.06.147
0169-4332/

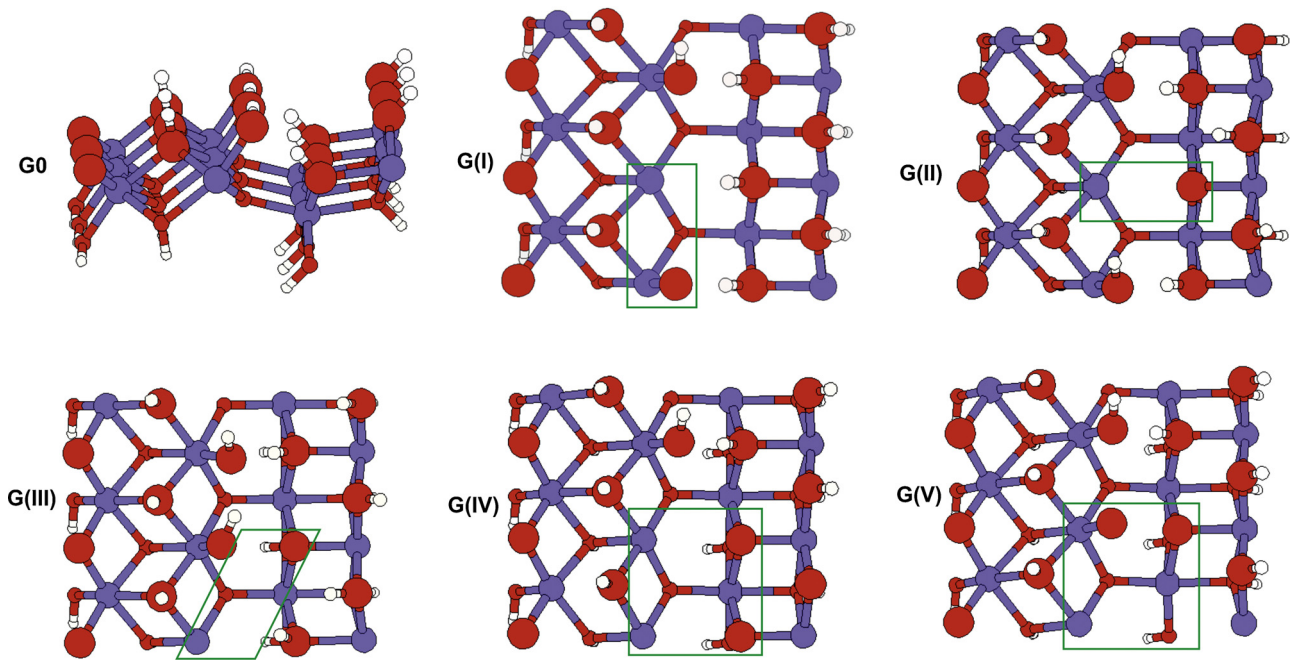


**Fig. 1.** Models of goethite surfaces used in the present work. Marked regions indicate the missing water molecules (violet = Fe, red = O, white = H). (For interpretation of the references to color in this figure legend, the reader is referred to the web version of the article.)

The aim of this work is to contribute to the understanding of the interaction between $SO_2$ and the α-FeOOH(1 1 0) surface. As we shall see later, this surface presents several types of hydroxyl groups, and hence different surface defects can be modeled by partial dehydration. A geometry search was performed to identify possible adsorbed $SO_2$ configurations and analyze their correlation with frequency vibrational values.

## 2. Computational details

The calculations were carried out in the framework of the density functional theory (DFT) using the Vienna Ab-initio Simulation Package (VASP) [15–17]. In this code, the Kohn–Sham equations are solved using plane wave basis sets. Electron exchange and correlation effects are described by the generalized gradient approximation (GGA) using the functional proposed by Perdew and Wang (PW91) [18,19]. A number of eight valence electrons for Fe atoms ($3d^7 4s^1$), six valence electrons for O atoms ($2s^2 2p^4$) and six valence electrons for S atom ($3s^2 3p^4$) were taken into account. The remaining (core) electrons together with the nuclei were described by pseudo-potentials in the framework of the projected augmented wave (PAW) method [20,21]. For H the ultrasoft PAW potential was used.

The two-dimensional Brillouin integrations were performed using a $(2 \times 3 \times 1)$ Monkhorst–Pack *k*-point grid [22]. The self-consistent field was considered converged when the forces on atoms were smaller than 0.01 eV/Å. The fixed convergence of the plane wave expansion was obtained with a cut-off energy of 450 eV. Spin-polarized GGA calculations were carried out for all adsorbate–surface systems.

The bulk goethite structure can be described as a distorted hexagonally close packing of O and OH groups with iron ions occupying half of the octahedral interstitial holes. For the construction of the FeOOH(1 1 0) surface, it was taken into account a previous study of the bulk goethite using the DFT + U approximation [23]. For magnetic materials such as FeOOH, where *d* electrons are strongly correlated, the standard DFT fails to predict their proper electronic ground state. A systematic study of several physical properties of bulk goethite was attained varying the value of the effective on-site repulsion term (U). In agreement with experimental results, the geometrical parameters, magnetic and elastic properties at the equilibrium were obtained using GGA + *U* with *U* = 6.0 eV. The unit cell parameters of the optimized bulk were *a* = 4.601, *b* = 9.994 and *c* = 3.035 Å, with an antiferromagnetic (AFM) arrangement, where each Fe ion is surrounded by other two with opposite magnetic moments along the *b*-vector axis of the bulk cell.

In natural and synthetic goethite it was established that the dominant face is the (1 1 0) surface (referred space group Pbnm) [24]. It was constructed by a stoichiometric truncation of the bulk using a $1 \times 3$ supercell and containing four Fe layers [25,26]. A vacuum gap in *z*-direction of approximately 15 Å was employed. In this partially dehydrated surface, three Fe—O and three O—H bonds per unit cell were broken from the bulk structure. From that surface, a fully hydrated surface was modeled by saturating all bonds (Fig. 1, indicated as G0). This hydrated surface presents three singly coordinated ($\mu_1$-OH), three doubly coordinated ($\mu_2$-OH), and six threefold coordinated ($\mu_3$-OH) hydroxyl groups per supercell with calculated Fe—OH distances of about 1.95, 2.0 and 2.1 Å, respectively.

A series of five different partially dehydrated surfaces were modeled by eliminating one or two water molecules from the fully hydrated surface, through the simultaneous releasing of adjacent OH and H (Fig. 1). We label these surface models with roman numbers, from G(I) to G(V). In G(I), G(II) and G(III), one $\mu_1$-OH group is eliminated together with different types of neighbor H atoms. In G(IV) and G(V), two water molecules are simultaneously released. While in G(IV) two adjacent $\mu_1$-OH are missing, in G(V) one $\mu_1$-OH and one $\mu_3$-OH are absent. These two last surfaces are deliberately modeled in order to allow the formation of sulfate complexes. The energies required for the formation of these vacant sites are calculated as the difference between the total energies of the partially dehydrated surface, and the energies of the G0 surface and the free water molecule(s). The calculated values are found to be 2.1, 1.7 and 3.4 eV for G(I), G(II) and G(III), respectively. For double vacancies, G(IV) and G(V), the values are 1.9 and 3.0 eV per water molecule, respectively. The large values calculated for G(III) and G(V) are in relation with the existence of a repulsive interaction between two

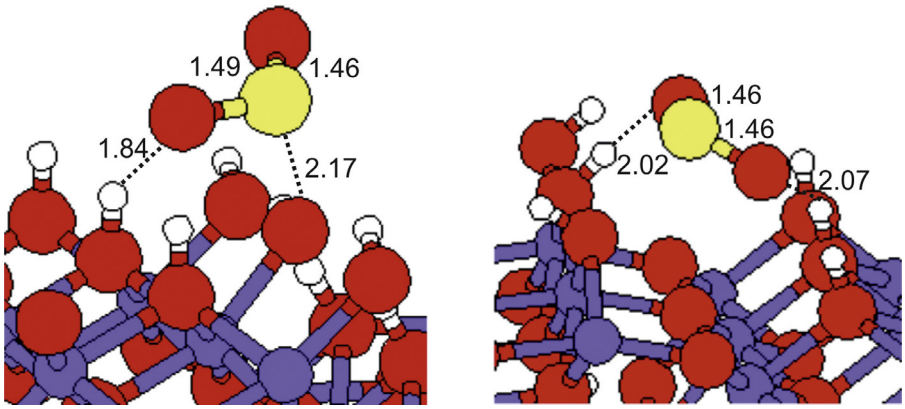


**Fig. 2.** Optimized structures of physisorbed $SO_2$ on hydrated goethite. Structure (I) on left panel and structure (II) on right panel (violet = Fe, red = O, white = H, yellow = S). (For interpretation of the references to color in this figure legend, the reader is referred to the web version of the article.)

nearby negatively charged O atoms on these surfaces. In the modeling, environmental dry conditions were taken into account; i.e., possible effects of other adsorbed water molecules or protonated surface hydroxyls on $SO_2$ adsorption were not considered.

Upon the DFT calculations, the adsorption energy ($E_{ads}$) of $SO_2$ molecule on goethite was defined as: $E_{ads} = E_{SO_2/FeOOH} - E_{FeOOH} - E_{SO_2}$, where $E_{SO_2/FeOOH}$ is the energy of the total system, $E_{FeOOH}$ is the bare surface energy and $E_{SO_2}$ is the energy of $SO_2$ in gas phase. Thus, negative values correspond to exothermic processes. As in all standard DFT studies, entropic effects are neglected. During the geometrical optimization procedure the position of all the surface hydroxyls, the six outermost Fe atoms and the atoms belonging to adsorbed $SO_2$ species are fully optimized. As initial geometry, the $SO_2$ molecule was located above the water vacancies (marked regions in Fig. 1). As mentioned above, the process of eliminating water molecules requires different energies and therefore $E_{ads}$ values depend on the corresponding model of goethite surface (the $E_{FeOOH}$ term). For this reason we used $E_{ads}$ values to analyze the relative stability of the different S-containing structures only when the same goethite surface model is used.

Considering that $SO_2$ can physisorb on the fully hydrated surfaces (see later), complementary calculations were performed using a van der Waals corrected-DFT approach. This is because it is well known that DFT does not correctly describe this type of long-range forces. The so-called DFT-D approximation was employed based on the addition of damped atom-pairwise dispersion corrections [27]. For comparison, one type of chemisorbed sulfite complex was also analyzed using the same methodology. The corresponding results are presented in the next section.

Vibrational frequency and atomic charges are also calculated for all the surface complexes. The vibrational frequencies and the corresponding normal modes were provided by the numerical calculation of the second derivatives of the potential energy surface within the harmonic approach. A geometrical displacement of 0.02 Å was used for all vibrational calculations. Local atomic charges have been calculated with the atoms-in-molecules-analysis developed by Bader [28] using the algorithm performed by Henkelman et al. [29,30].

## 3. Results and discussion

### 3.1. Physisorbed $SO_2$

The optimized $SO_2$ structures adsorbed on the fully hydrated FeOOH surface are shown in Fig. 2, and the corresponding adsorption energies and frequency values are summarized in Table 1. Two different geometries were found, indicated as (I) and (II), with very similar adsorption energies, −0.58 and −0.57 eV, respectively. In the first case, a hydrogen bond is formed between an O atom of $SO_2$ and a H atom belonging to $\mu_3$-OH. Consequently, this S—O link is elongated from 1.45 Å, the distance at free $SO_2$, to 1.49 Å. The other O atom of $SO_2$ is tilted away from the surface. The adsorbed molecule is also stabilized by the formation of a relatively short S···O bond, 2.17 Å. The second mode results from the interaction of $SO_2$ with $\mu_2$-OH and $\mu_3$-OH hydroxyls, forming two hydrogen bonds of 2.02 and 2.07 Å, respectively. In this case, the S atom is far from the surface (S···O distance being 2.50 Å) and both S—O bonds are slightly elongated to 1.46 Å. Lo et al. have found similar structures upon $SO_2$ adsorption on a hydrated $\gamma$-$Al_2O_3$(1 1 0) surface by using periodic DFT [12] but with larger adsorption energies, of around 1 eV. In one of these structures, one O atom of $SO_2$ is close to the surface and other one pointed out form the surface, with a S···O bond of 2.28 Å; in the other configuration, the $SO_2$ molecule is approximately parallel to the surface with a S···O distance of 2.52 Å.

Gas-phase $SO_2$ molecule presents three characteristic vibrational modes calculated at 1368, 1175 and 493 $cm^{-1}$, attributed to asymmetric/symmetric stretching and bending modes, respectively. In structures (I) and (II), while the bending mode is slightly modified, the stretching asymmetric/symmetric modes decrease by about 150–170 and 100–150 $cm^{-1}$, respectively. The longer S—O distance in structure (I), correlates with the corresponding lower values of stretching modes (Table 1). Bader population analysis indicates a slight charge transfer from the surface to $SO_2$; for structures (I) and (II) we have computed a net $SO_2$ charge of −0.1 and −0.2*e*, respectively. From IR measurements, Kaneko and Matsumoto have detected a weak peak at 1038 $cm^{-1}$ during $SO_2$ adsorption on goethite that they assigned to negatively charged $SO_2$ [8], in line with our calculated values of 1029 and 1069 $cm^{-1}$ due to $\nu_s$OSO stretching mode.

### 3.2. Surface sulfite species

Six stable forms of surface sulfite have been identified (Fig. 3). Both types of partially dehydrated goethite surfaces (with one or two missing water molecules) can produce sulfite structures. We found two monodentate mononuclear configurations, indicated by MdMn(I) and MdMn(II), and four bidentate (Bd) structures. These latter geometries can be binuclear, indicated as BdBn(I) and BdBn(II), or polinuclear, labeled as BdPn(I) and BdPn(II). In BdPn complexes, one O of sulfite is singly coordinated and the other one is threefold coordinated with Fe ions.

In MdMn structures, the S—$O_{Fe}$ distance is longer than the other S—O ones. Besides, one of the three oxygen atoms belonging to sulfite presents a hydrogen bond with O···H distances of 1.72 and

**Table 1**
Calculated adsorption energies and vibrational frequencies of adsorbed $SO_2$ on FeOOH(1 1 0).

| Adsorption mode | Goethite slab | $E_{ads}$ (eV) | Frequencies ($cm^{-1}$) |
|---|---|---|---|
| Physisorbed $SO_2$ (I) | G0 | −0.58 | 1194 ($\nu_{as}$OSO), 1029 ($\nu_s$OSO), 520 (δOSO) |
| Physisorbed $SO_2$ (II) | G0 | −0.57 | 1221 ($\nu_{as}$OSO), 1069 ($\nu_s$OSO), 501 (δOSO) |
| Sulfite MdMn(I) | G(I) | −1.59 | 1126 ($\nu_{as}$OSO), 976 ($\nu_{as}OSO_{Fe}$), 648 ($\nu_s OSO_{Fe}$), 593 ($\delta OSO_{Fe}$) |
| Sulfite MdMn(II) | G(V) | −2.62 | 1126 ($\nu_{as}$OSO), 977 ($\nu_{as}OSO_{Fe}$), 868 ($\nu SO_{Fe}$), 541 ($\delta OSO_{Fe}$) |
| Sulfite BdBn(I) | G(I) | −2.50 | 1022 (νSO), 791 ($\nu_s O_{Fe}SO_{Fe}$), 672 ($\nu_{as}O_{Fe}SO_{Fe}$), 578 ($\delta OSO_{Fe}$) |
| Sulfite BdBn(II) | G(V) | −3.48 | 1049 (νSO), 809 ($\nu SO_{Fe}$), 661 ($\nu_{as}O_{Fe}SO_{Fe}$), 530 ($\delta OSO_{Fe}$) |
| Sulfite BdPn(I) | G(II) | −1.66 | 1056 (νSO), 904 ($\nu SO_{Fe}$), 553 ($\delta OSO_{Fe}$), 522($\delta OSO_{Fe}$) |
| Sulfite BdPn(II) | G(IV) | −1.99 | 1058 (νSO), 873 ($\nu SO_{Fe}$), 561 δ($OSO_{Fe}$), |
| Bisulfite | G(III) | −2.29 | 1111 (νSO), 1087 ($\nu_{as}$OSO), 1011 ($\nu_s$OSO), 564 ($\delta OSO_{Fe}$), 539 ($\delta OSO_{Fe}$) |
| Sulfate | G(IV)<br>G(V) | −2.27<br>−5.02 | 1176 ($\nu_{as}$OSO), 1029 ($\nu_{as}OSO_{Fe}$), 918 ($\nu_s$OSO), 791($\nu SO_{Fe}$), 602 ($\delta OSO_{Fe}$), 583 (δOSO), 540 ($\delta OSO_{Fe}$) |

1.77 Å for MdMn(I) and for MdMn(II), respectively. Concerning the BdBn structures, both of them present similar geometries with two S—$O_{Fe}$ distances of about 1.6 Å. In BdPn, the two S—$O_{Fe}$ distances are very different, one relatively short of about 1.56 Å and the other one much longer (1.78 and 1.73 Å for BdPn(I) and BdPn(II), respectively). On the other hand, BdBn states show short hydrogen bonds at 1.69 and 1.64 Å. BdPn present somewhat longer hydrogen bonds, about 1.7 Å.

Nearly in all the structures, the Fe—$O_S$ distance is around 2 Å, indicating a strong bonding with the surface. The only exceptions are the distances with the three-coordinated O present at both BdPn configurations, with larger values of about 2.2 Å.

It is interesting to note that MdMn(I) and BdBn(I) are formed on G(I), and MdMn(II) and BdBn(II), on G(V). Besides, for each case, adsorption energy values are 0.9 eV more stable for BdBn due to the double anchorage with the surface.

Both MdMn geometries present two frequency values at 1126 and 976 $cm^{-1}$ corresponding to OSO and $OSO_{Fe}$ asymmetric stretching modes, respectively. The longer S—$O_{Fe}$ in MdMn(I) in comparison with (II) is reflected in the corresponding stretching modes; indeed, a band at 648 $cm^{-1}$ appears in (I), associated to symmetric $OSO_{Fe}$, and another one is present in (II) but at higher frequencies (868 $cm^{-1}$) because it involves a shorter distance (1.55 Å).

Both BdBn states present very similar frequencies. It is interesting to note that the features at 672 and 661 $cm^{-1}$, together with the value of 648 $cm^{-1}$ corresponding to MdMn(I), are distinctive of these sulfite geometries. Indeed, neither of the other structures presented here show values in the range between 600 and 700 $cm^{-1}$. In general, the FTIR spectra are recorded from 700 $cm^{-1}$ to higher values and that is why bands within the 600–700 $cm^{-1}$ range were not previously reported.

Concerning the bidentate polinuclear configurations, we can see that BdPn(I) presents a higher value of the $SO_{Fe}$ stretching in comparison with the same mode present in (II) (904 and 873 $cm^{-1}$, respectively) owing to the longer S—$O_{Fe}$ distance at (I).

On the other hand, considering all the sulfite structures, bending modes vary in a rather narrow range, between 522 and 593 $cm^{-1}$. These adsorption bands are usually very weak and hence rarely reported.

IR studies performed by Kaneko and Matsumoto [8] show two main adsorption bands at 940 and 850 $cm^{-1}$ that they assigned to

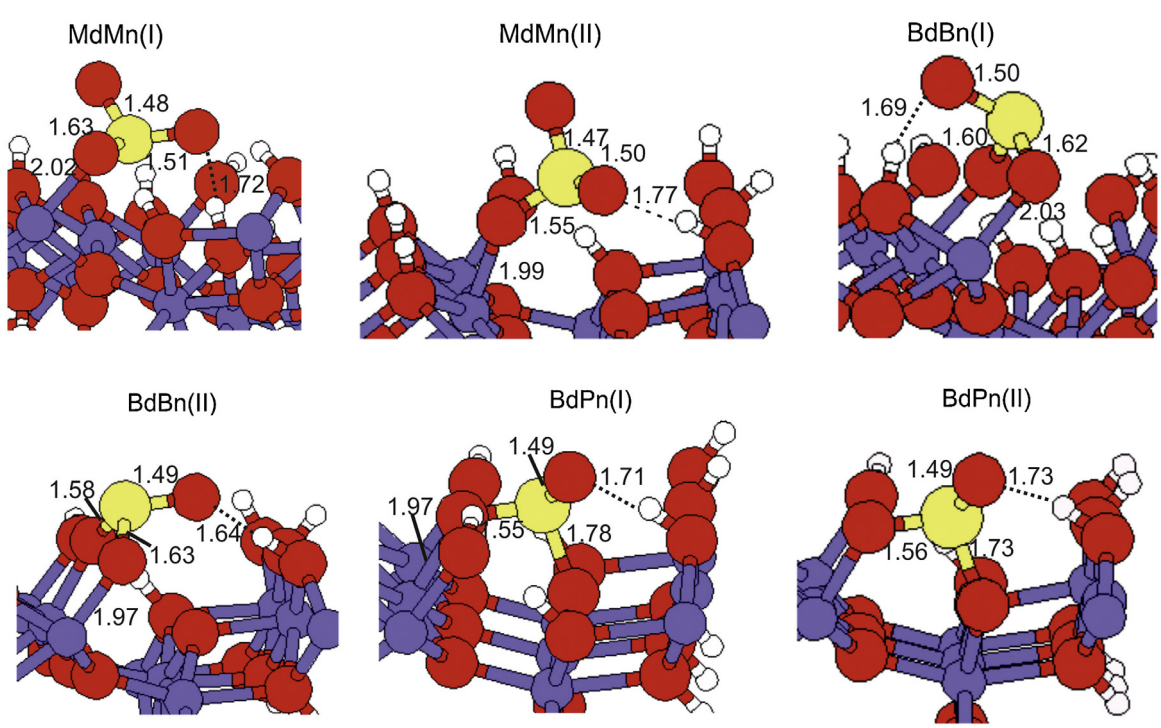


**Fig. 3.** Optimized structures of surface sulfite species on dehydrated goethite (violet = Fe, red = O, white = H, yellow = S). (For interpretation of the references to color in this figure legend, the reader is referred to the web version of the article.)

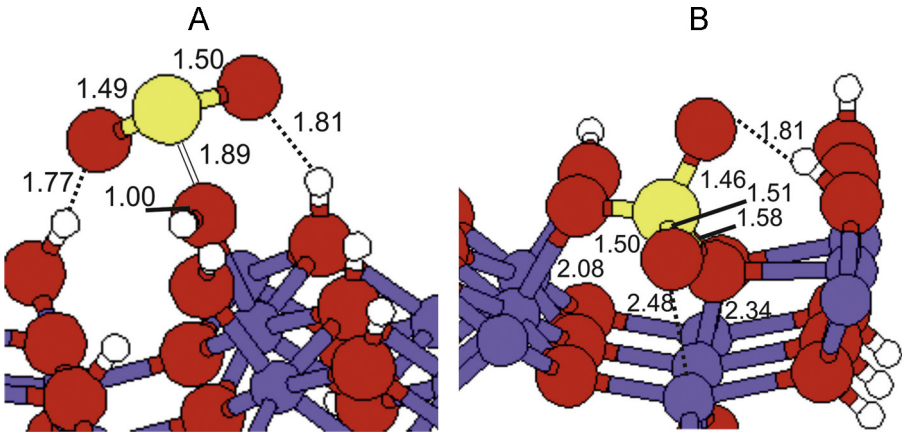


**Fig. 4.** (A) Optimized structure of surface bisulfite species on dehydrated goethite (violet = Fe, red = O, white = H, yellow = S). (B) Optimized structure of surface sulfate species on dehydrated goethite (violet = Fe, red = O, white = H, yellow = S). (For interpretation of the references to color in this figure legend, the reader is referred to the web version of the article.)

"—$OSO_2$" species on goethite. Some of the sulfite-like complexes obtained in our models give similar values. Indeed, both MdMn structures present features at 977 $cm^{-1}$ due to stretching OSO. Besides, MdMn(II) and BdPn(II) present bands at 868 $cm^{-1}$ and 873 $cm^{-1}$, respectively, due to $SO_{Fe}$ stretching mode.

Bader analysis shows that all the sulfite complexes present a net charge of the $SO_3$ group of about −1.4*e*.

### 3.3. Surface bisulfate species

Only the adsorption on the G(III) yields to the spontaneous formation of a bisulfite-like structure, via bonding between S and an O atom belonging to $\mu_1$OH. Two hydrogen bonds contribute also to its stabilization. As we can see in Fig. 4A, one of the S—O distances is much longer than the others. This geometry is not possible on the fully hydrated goethite very likely due to steric effects. Lo et al. have found a similar structure on alumina surfaces using periodic DFT [12]. Bader analysis shows a net charge of the $HSO_3$ complex of −0.8*e*.

Experimentally, the same IR adsorption range is assigned to the features owing to sulfite and bisulfate species. For instance, Zhang et al. have assigned a broad band between 850 and 1100 $cm^{-1}$ observed in IR spectra to bisulfite and sulfite complexes obtained during $SO_2$ adsorption on alumina [4]. Goodman et al. have attributed a band between 900 and 1200 $cm^{-1}$ to bisulfate and sulfites also on alumina [14]. In comparison, we have found signals at the upper limits of those ranges for bisulfate, between 1011 and 1111 $cm^{-1}$.

### 3.4. Surface sulfate species

The sulfate structure is formed on G(IV) and G(V) surface models, giving exactly the same structure (Fig. 4B). The adsorption energy was calculated as −2.29 and −5.02 for G(IV) and G(V), respectively. The large value in the latter case is in relation with the above mentioned relative instability of the G(V) surface. As seen in Table 1, sulfite MdMn(II) and BdBn(II) complexes are also formed on this surface; the adsorption energies follow the sequence (in magnitude) sulfate > sulfite BdBn(II) > sulfite MdMn(II), as expected taking into account the number of links with the goethite surface.

The sulfate species has two O singly coordinated and one O threefold coordinated with Fe ions. The O—Fe distances are 2.08, 2.34 and 2.48 Å, and for this reason it could be associated with a tridentate geometry. As shown in the figure, a relatively long hydrogen bond is also formed. The calculated charge for the $SO_4$ group is −1.6*e*.

Using IR spectroscopy, Fu et al. [6] have detected three main peaks at 1203, 1145 and 1042 $cm^{-1}$ attributed to bidentate sulfate formed on goethite, together with a weak peak at 994 $cm^{-1}$. Our calculations show three bands in the same range, at 1176, 1029 and 918 $cm^{-1}$ due to asymmetric OSO, asymmetric $OSO_{Fe}$, and symmetric OSO stretching modes of the sulfate structure, respectively. Besides, our model predicts a feature at lower frequencies, 791 $cm^{-1}$, owing to $SO_{Fe}$ stretching. We can tentatively assign the calculated values at 1176, 1029 and 918 $cm^{-1}$ to the bands experimentally recorded at 1203, 1042 and 994 $cm^{-1}$. The band at 1145 $cm^{-1}$ may be associated to sulfite structures, for instance, those at 1126 $cm^{-1}$ corresponding to SO stretching modes at sulfite MdMn species. In fact, as mentioned above, XPS experiments show that sulfite complexes are the predominant species upon $SO_2$ adsorption on goethite, even in the presence of oxygen [7]. Thus, sulfate and sulfite species could be simultaneously present in the reported IR spectrum [6], and not only bidentate sulfate.

As mentioned above, we have tested the effect of including the dispersion forces using a corrected DFT methodology. For that, we have used the PBE functional with a fitted empirical term to account for the dispersion interactions [27]. We have chosen two different adsorption modes: physisorbed $SO_2$ (structure II) and sulfite BdBn(I). Calculations indicate that the adsorption energies increased by about 0.2 eV in magnitude. Concretely, $E_{ads}$ resulted to be −0.77 and −2.75 eV for physisorbed $SO_2$ and sulfite BdBn(I), respectively. In relation with the optimized geometries, while the S—O distances change slightly, less than 0.01 Å, hydrogen bonds between surface hydroxyls and the O of $SO_2$ vary around 0.03 Å. Frequency values increase by about 9 $cm^{-1}$ at the most, for both stretching and bending modes. We thus observed that the inclusion of the dispersion forces correction does not seem to modify the general trends and the main conclusions obtained using non-corrected DFT.

It is important to take into account that the results presented here are concerned with the $SO_2$ adsorption on goethite exposing only the (1 1 0) face, while the experimental data are obtained from synthetic goethite samples where more than one crystallographic plane are exposed. Villalobos et al. have recently found that other surfaces such as (0 2 1), apart from the (1 1 0) one, are very reactive to different adsorbates [31,32]. Therefore, other surfaces may have a great affinity toward $SO_2$ adsorption. Besides, adsorbed $SO_2$ could show different frequency values according to the exposed surface. For instance, changes in the band positions recently observed in IR spectra upon phosphate adsorption on microgoethite and nanogoethite samples could be attributed, at least in part, to the variations in different exposing facets [33]. Thus, further

investigations on other surfaces are needed to acquire a complete theoretical description of the $SO_2$–goethite interface.

## 4. Conclusions

The adsorption of $SO_2$ on hydrated and partially dehydrated goethite was evaluated. A series of five different dehydrated surfaces were modeled by eliminating one or two water molecules. On the hydrated surface, $SO_2$ adsorbs molecularly through the formation of S···O and hydrogen bonds. Most of the hydrated surface models give rise to sulfite species, with both monodentate and bidentate structures. Only one of our models yields to the formation of bisulfite, via bonding between the S atom and an O atom belonging to $\mu_1$OH. On the other hand, $SO_2$ transforms into sulfate species on the surfaces with two missing water molecules.

Bader charges of $SO_x$ species follow the sequence $SO_4$ $(-1.6e) > SO_3$ $(-1.4e) > HSO_3$ $(-0.8e) >$ physisorbed $SO_2$ $(-0.1/-0.2e)$.

The frequency values for monodentate mononuclear sulfite structures calculated at 977 $cm^{-1}$ (asymmetric OSO stretching) and 868 $cm^{-1}$ due to ($SO_{Fe}$ stretching) agree quite well with two adsorptions bands at 940 and 850 $cm^{-1}$ observed using IR spectroscopy. For sulfate, the calculated values obtained at 1176, 1029 and 918 $cm^{-1}$ due to asymmetric OSO, asymmetric $OSO_{Fe}$, and symmetric OSO stretching modes of the sulfate structure, respectively, are also in line with reported IR spectra. It is interesting to note that features at around 660 $cm^{-1}$, found for several sulfite geometries, are distinctive of these structures because neither of the other species shows values in the 600–700 $cm^{-1}$ range (usually not explored in IR experiments). Taking into account that all the $SO_x$ structures analyzed here present bands in the same range, between 800 and 1250 $cm^{-1}$, the predicted bands falling into the 600–700 $cm^{-1}$ region can be used in future measurements for the detection of sulfite species.

## References


[1] R.M. Cornell, U. Schwertmann, The Iron Oxides: Structure, Properties, Reactions, Occurrences and Uses, Wiley-Vch, Weinheim, 2003.
[2] M.J.D. Low, A.J. Goodsel, N. Takezawa, Reactions of gaseous pollutants with solids. I. Infrared study of the sorption, Environ. Sci. Technol. 5 (1997) 1191–1195.
[3] D.S. Toledano, V.E. Henrich, Kinetics of $SO_2$ adsorption on photoexcited $\alpha$-$Fe_2O_3$, J. Phys. Chem. B 105 (2001) 3872–3877.
[4] X. Zhang, G. Zhuang, J. Chen, Y. Wang, X. Wang, Z. An, P. Zhang, Heterogeneous reactions of sulfur dioxide on typical mineral particles, J. Phys. Chem. B 110 (2006) 12588–12596.
[5] H.G. Karge, I.G. Dalla Lana, Infrared studies of $SO_2$ adsorption on a Claus catalyst by selective poisoning of sites, J. Phys. Chem. 88 (1984) 1538–1543.
[6] H. Fu, X. Wang, H. Wu, Y. Yin, J. Chen, Heterogeneous uptake and oxidation of $SO_2$ on iron oxides, J. Phys. Chem. C 111 (2007) 6077–6085.
[7] J. Baltrusaitis, D.M. Cwiertny, V.H. Grassian, Adsorption of sulfur dioxide on hematite and goethite particle surfaces, Phys. Chem. Chem. Phys. 9 (2007) 5542–5554.
[8] K. Kaneko, A. Matsumoto, Role of surface defects in the chemisorption of NO and $SO_2$ on variable-sized crystalline $\alpha$-FeOOH, J. Phys. Chem. 93 (1989) 8090–8095.
[9] H. Fu, T. Xu, S. Yang, S. Zhang, J. Chen, Photoinduced formation of Fe(III)-sulfato complexes on the surface of $\alpha$-$Fe_2O_3$ and their photochemical performance, J. Phys. Chem. C 113 (2009) 11316–11322.
[10] M.B. Mitchell, V.N. Sheinker, M.G. White, Adsorption and reaction of sulfur dioxide on alumina and sodium-impregnated alumina, J. Phys. Chem. 100 (1996) 7550–7557.
[11] L. Zhao, X. Li, C. Hao, C.L. Raston, $SO_2$ adsorption and transformation on calcined NiAl hydrotalcite-like compounds surfaces: an in situ FTIR and DFT study, Appl. Catal. B: Environ. 117–118 (2012) 339–345.
[12] J. Lo, T. Ziegler, P. Clark, $SO_2$ adsorption and transformations on $Al_2O_3$ surfaces. A density functional theory study, J. Phys. Chem. C 114 (2010) 10444–10454.
[13] Q. Wu, H. Gao, H. He, Conformational analysis of sulfate species on Ag/$Al_2O_3$ by means of theoretical and experimental vibrational spectra, J. Phys. Chem. B 110 (2006) 8320–8324.
[14] A.L. Goodman, P. Li, C.R. Usher, V.H. Grassian, Heterogeneous uptake of sulfur dioxide on aluminum and magnesium oxide particles, J. Phys. Chem. A 105 (2001) 6109–6120.
[15] G. Kresse, J. Hafner, Ab initio molecular dynamics for liquid metals, Phys. Rev. B 47 (1992) 558–561.
[16] G. Kresse, J. Hafner, Ab initio molecular dynamics for open-shell transition metals, Phys. Rev. B 48 (1993) 13115–13118.
[17] G. Kresse, J. Hafner, Ab initio molecular-dynamics simulation of the liquid-metal-amorphous-semiconductor transition in germanium, Phys. Rev. B 49 (1994) 14251–14269.
[18] J.P. Perdew, J.A. Chevary, S.H. Vosko, K.A. Jackson, M.R. Pederson, D.J. Singh, C. Fiolhais, Atoms, molecules, solids, and surfaces: applications of the generalized gradient approximation for exchange and correlation, Phys. Rev. B 46 (1992) 6671–6687.
[19] J.P. Perdew, J.A. Chevary, S.H. Vosko, K.A. Jackson, M.R. Pederson, D.J. Singh, C. Fiolhais, Atoms, molecules, solids, and surfaces: applications of the generalized gradient approximation for exchange and correlation, Phys Rev. B 48 (1993) 4978.
[20] P. Blochl, Projector augmented-wave method, Phys. Rev. B 50 (1994) 17953–17979.
[21] G. Kresse, D. Joubert, From ultrasoft pseudopotentials to the projector augmented-wave method, Phys. Rev. B 59 (1999) 1758–1775.
[22] H.J. Monkhorst, J.D. Pack, On special points for brillouin zone integrations, Phys. Rev. B 13 (1976) 5188–5192.
[23] S.A. Fuente, P.G. Belelli, N.J. Castellani, M. Avena, LDA+U and GGA+U studies of Al-rich and bulk goethite, Mater. Chem. Phys. 137 (2013) 1012–1020.
[24] U. Schwertmann, U.R.M. Taylor, in: J.B. Dixon, S.B. Weed (Eds.), Minerals in Soil Environments, 2nd ed., Soil Science Society of America, Madison, WI, 1989, pp. 379.
[25] B. Russell, M. Payne, L. Colombi Ciacchi, Density functional theory study of Fe(II) adsorption and oxidation on goethite surfaces, Phys. Rev. B 79 (2009) 165101.
[26] P.G. Belelli, S.A. Fuente, N.J. Castellani, Phosphate adsorption on goethite and Al-rich goethite, Comput. Mater. Sci. 85 (2014) 59–66.
[27] S. Grimme, Semiempirical GGA-type density functional constructed with a long-range dispersion correction, J. Comput. Chem. 27 (2006) 1787–1799.
[28] R.F.W. Bader, Atoms in Molecules: A Quantum Theory;, Oxford Science, Oxford, UK, 1990.
[29] G. Henkelman, A. Arnaldsson, H. Jónsson, A fast and robust algorithm for Bader decomposition of charge density, Comput. Mater. Sci. 36 (2006) 254–360.
[30] E. Sanville, S.D. Kenny, R. Smith, G. Henkelman, Improved grid-based algorithm for Bader charge allocation, J. Comp. Chem. 28 (2007) 899–908.
[31] M. Villalobos, A. Pérez-Gallegos, Goethite surface reactivity: a macroscopic investigation unifying proton, chromate, carbonate and lead(II) adsorption, J. Colloid Interface Sci. 326 (2008) 307–323.
[32] M. Villalobos, M.A. Cheney, J. Alcaraz-Cienfuegos, Goethite surface reactivity: II. A microscopic site-density model that describes its surface area-normalized variability, J. Colloid Interface Sci. 336 (2009) 412–422.
[33] J.D. Kubicki, K.W. Paul, L. Kabalan, Q. Zhu, M.K. Mrozik, M. Aryanpour, A. Pierre-Louis, D.R. Strongin, ATR–FTIR and density functional theory study of the structures, energetics, and vibrational spectra of phosphate adsorbed onto goethite, Langmuir 28 (2012) 14573–14587.